Journal of Crystal Growth 452 (2016) 263–267

Contents lists available at ScienceDirect

Journal of Crystal Growth

journal homepage: www.elsevier.com/locate/jcrysgro

Sensitivity of quantum cascade laser performance to thickness and doping variations ☆

D.F. Siriani [a,*], C.A. Wang [a], J.P. Donnelly [a], M.K. Connors [a], L.J. Missaggia [a], D.R. Calawa [a], D. McNulty [a], M.C. Zheng [a], T.S. Mansuripur [b], F. Capasso [b]

[a] Lincoln Laboratory, Massachusetts Institute of Technology, Lexington, MA 02420, USA
[b] John A. Paulson School of Engineering and Applied Sciences, Harvard University, Cambridge, MA 02138, USA

ARTICLE INFO

Communicated by C. Caneau
Available online 23 November 2015

Keywords:
A3. Metalorganic vapor phase epitaxy
B2. Semiconducting III–V materials
B3. Infrared devices
B3. Quantum cascade lasers

ABSTRACT

We report on a study of the effects of intentional thickness and doping variations on QCL performance. The measured QCL data had very similar trends to those predicted by an in-house QCL model. It was found that absolute changes to the QCL period had a very small effect on emission wavelength (wavelength/period change <10 nm/Å), whereas the complementary thickness changes between the wells and barriers had a large effect (wavelength/thickness change$=550$ nm/Å). The threshold voltage also changed with these variations and generally agreed well with the model. We show through modeling and experiments that intentional structure variations can have largely different magnitudes of effect on QCL performance.

1. Introduction

Quantum cascade lasers (QCLs) [1] are coherent optical sources capable of room temperature, continuous wave operation over a broad bandwidth in the mid-wave infrared (MWIR, 3–7 μm) and long-wave infrared (LWIR, 8–12 μm) wavelength ranges. This aspect makes them appealing for applications in infrared countermeasures, spectroscopy, chemical and biological sensing, and free-space optical communications. The flexible wavelengths of QCLs are achievable because the optical transition energy is determined by the energy separation of subband states in the conduction band of a coupled quantum-well structure. The energy-level separation is determined by the thicknesses of the many quantum wells and barriers in the structure, which typically can number more than 20 layers with some layers only a few monolayers thick. As such, there is potential for unintentional growth variations to produce significant differences between the intended and physically realized QCL structure. For example, a 6% reduction in QCL wavelength from the designed 8.1 μm wavelength has been attributed to a 5% reduction in layer thicknesses [2]. While there have been numerous studies on the growth optimization of QCLs, those studies have focused mainly on growth conditions such as temperature, growth rate, V/III ratio, and growth interrupts [3–8,10].

This work reports the study of the effects of layer thickness and doping variations on the performance of QCLs grown by OMVPE. As explored in other work, OMVPE growth of QCL material in a step-flow growth mode is sensitively dependent on growth conditions, many of which can affect the actual as-grown QCL structure [4,5,7,8]. Different types of thickness changes were intentionally incorporated throughout the QCL structure to understand some potential growth variations, such as effects of evolving or miscalibrated growth rates. Moreover, doping in the injector region and the thickness of the injection barrier were altered to witness their effects on carrier transport. All grown structures were characterized under pulsed conditions; electroluminescence and current–light–voltage data were collected on fabricated mesa structures and ridge lasers, respectively. In order to determine if the growth effects on performance could be predicted, experimental results were compared to calculations from an in-house model. This study shows that different growth variations can have orders of magnitude difference in changes to QCL properties, such as wavelength and current transport.

2. Experimental procedure

The lattice-matched AlInAs/GaInAs QCL structures were grown on (100) InP substrates by organometallic vapor phase epitaxy (OMVPE) in a Veeco D125 multi-wafer reactor. Trimethylaluminum

☆This work is sponsored by the Assistant Secretary of Defense for Research& Engineering under Air Force Contract FA8721-05-C-0002. Opinions, interpretations, conclusions and recommendations are those of the author and are not necessarily endorsed by the United States Government.

* Corresponding author. Tel.: +1 781 981 5858.
E-mail address: dominic.siriani@LL.mit.edu (D.F. Siriani).

http://dx.doi.org/10.1016/j.jcrysgro.2015.11.006
0022-0248/

(TMAl), trimethylindium (TMIn), trimethylgallium (TMGa), phosphine (PH_3), and arsine (AsH_3) were used as precursors and disilane (Si_2H_6) was the n-type dopant, as described previously [9]. H_2 was used as the carrier gas. The growth temperature was 625° C, and the growth rate was ~0.3 nm/s for both AlInAs and GaInAs. The InP cladding was grown at a higher rate of 0.6–0.7 nm/s. No growth interrupts were used. The V/III ratios were ~90 for AlInAs and GaInAs, and ~130 for InP. The structures were characterized by high-resolution x-ray diffraction (HRXRD) to determine the average alloy composition and the QCL period.

A nominal 8.6 μm QCL structure based on single-phonon-continuum transport was used as the baseline [11]. The injector/active region is composed of nominally lattice-matched $Al_{0.48}$ InAs and $Ga_{0.47}$ InAs on InP, and consists of the following layers: **3.8** / 1.5 / **0.9** / 5.3 / **0.8** / 5.2 / **0.9** / 4.8 / **1.6** / 3.7 / **2.2** / 3.0 / **1.8** / 2.8 / **1.9** / 2.7 / **2.0** / 2.6 / **2.5**/ 2.7 / **3.1** / 2.5. The AlInAs barrier layers are in bold print, and the underlined layers are Si-doped injector layers. The injector doping was 8×10^{10} cm^{-2}. The lower and upper InP cladding layer thickness was 3.5 μm, and was Si doped 5×10^{16} cm^{-3}. GaInAs waveguide layers were Si doped 2×10^{16} cm^{-3} and were 0.5 μm thick. A heavily Si-doped ($>5\times$ 10^{18} cm^{-3}) plasmon-confinement layer was 0.5 μm thick.

Two separate studies were performed using this structure. In the first, a full QCL structure with a waveguide was grown, and layer thicknesses throughout the entire 35-period structure were changed uniformly. In this case, either the entire period of the QCL was increased or decreased by making all layers thicker or thinner by 5%, or the period was maintained by making complementary changes in the thickness of each barrier and well layers in steps of 0.5 Å. The samples are summarized in Table 1. In this study, the epitaxial material was fabricated into ridge waveguide lasers and mesa structures.

In the second study, a simplified 20-period structure without the waveguide was grown, and only the thickness of the injection barrier (thick barrier separating the injection and active regions) was varied by ± 10 Å and/or the doping was changed by $\pm 5 \times 10^{16}$ cm^{-3} from the nominal values of 38 Å and 1.0×10^{17} cm^{-3}, respectively. In particular, injection barrier thickness was varied in order to see the effects on current transport as predicted by resonant tunneling models [12–14]. The samples from this second study are summarized in Table 2; the epitaxial material was fabricated into circular mesa structures.

Standard photolithography and wet etching techniques were used to fabricate ridge lasers and mesa test structures. Ti–Au metallization was used for topside and backside contacts. The ridge lasers were of variable ridge widths from 10 μm to 25 μm in 5 μm steps. These devices were cleaved into 3-mm-long bars and tested as lasers with uncoated facets. The mesa structures had diameter of 200 μm.

The lasers were probe tested in chip form on a temperature-controlled stage held at 15 °C under pulsed operation (100–200 ns pulses at 10 kHz). Using this setup, current–voltage–power characteristics of the QCLs were collected. The mesas from the first study were cleaved in half; wavelength measurements of devices under bias were then taken using a FTIR spectrometer. The mesa from the second study were characterized using a similar pulsed operation setup as for the lasers, but only current–voltage information was gathered.

Table 1
Summary of samples of study 1.

Sample	Designed period (%)	Designed AlInAs/GaInAs (Å)	Measured period (%)
19	0	0/0	0
21	−5	0/0	−3.3
23	0	+1.0/−1.0	+5.0
25	0	+0.5/−0.5	+2.0
27	+5	0/0	+4.0
29	0	−0.5/+0.5	−0.7

Table 2
Summary of samples of study 2.

Sample	Inj. barrier change (Å)	Doping change (cm^{-3})	Measured period (%)
69	0	0	−0.2
70	+10	0	−0.5
78	+10	+5e16	+0.5
79	−10	+5e16	+0.4
80	+10	−5e16	+0.8
81	−10	−5e16	+0.9
82	0	−5e16	−0.2
83	−10	0	−0.5
84	0	0	−1.4
85	0	+5e16	−0.7

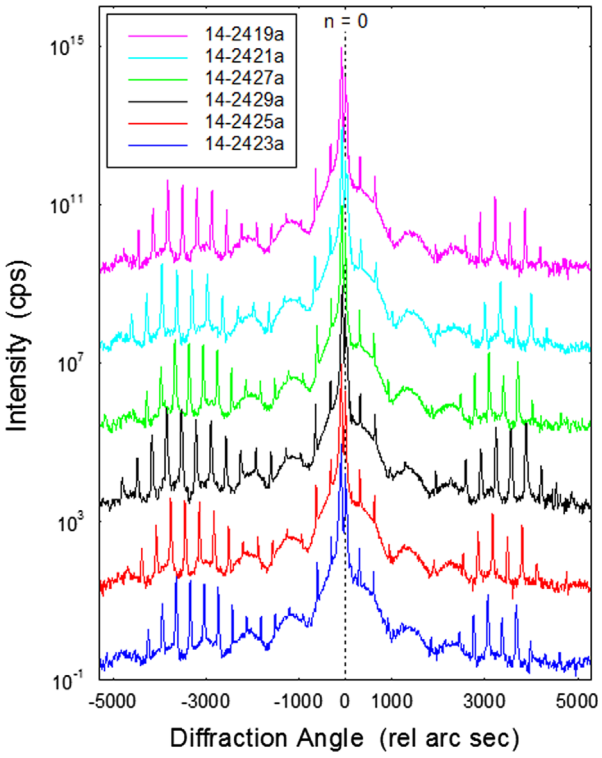

Fig. 1. High-resolution x-ray diffraction of AlInAs/GaInAs QCL structures from Table 1.

3. Results

3.1. Growth summary

High-resolution x-ray diffraction scans for the growths represented in Table 1 are shown in Fig. 1. The sharp satellite peaks and highly resolved interference fringes are indicative of excellent reproducibility of the QCL period. Moreover, the consistent location of the $n=0$ peak is telling of consistent growth from run-to-run and the desired lattice matching. Using the spacing of the satellite peaks in the x-ray data, the actual periods of the QCL structures were deduced. The difference between the measured period and that of the control sample (layer structure given above) are included in the final column of Table 1. The differences between desired and actual period thicknesses are attributed to an increase in growth rate over time due to deposition in the reactor. Similarly, the same measurements were performed for the study 2 growths and measured periods are included in Table 2. In this

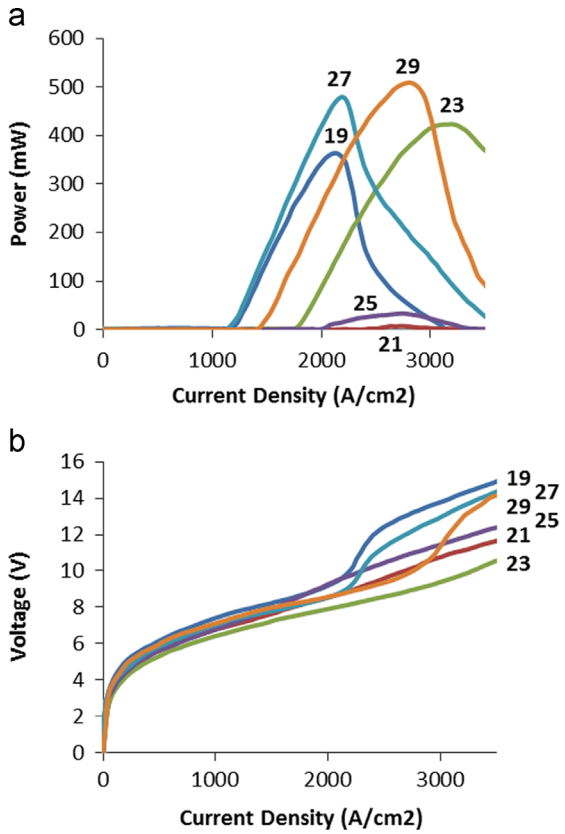

Fig. 2. Data from the QCLs of study 1. (a) Total output power from both facets as a function of current density and (b) applied voltage versus current density. The different sample numbers corresponding to the summary in Table 1 are labeled using their final two digits.

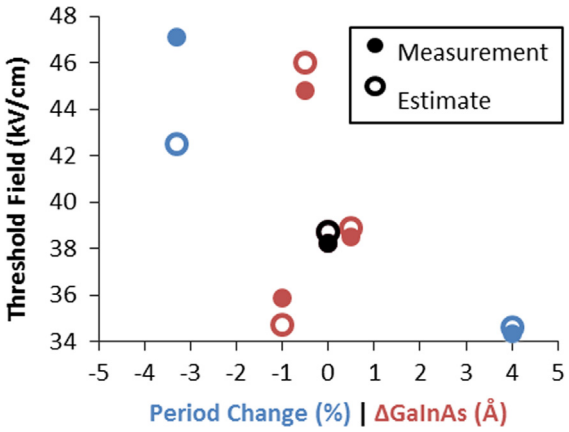

Fig. 3. Comparison of the threshold field (applied field at which laser turns on) as measured and calculated for different thickness changes. Blue points represent data from QCLs designed with a period thickness change (in %), red points represent data from QCLs designed with the complementary well and barrier thickness changes (in Å, and black points represent the control data). (For interpretation of the references to color in this figure caption, the reader is referred to the web version of this paper.)

case, the growth rate variation over time was compensated by appropriately adjusting growth parameters, and resultantly the actual and targeted period are very close.

3.2. Study 1 QCL devices

Pulsed light–current (LI) and voltage–current (VI) characteristics of the QCL devices summarized in Table 1 are shown in Fig. 2. All the devices have a ridge width of 25 μm and cavity length of 3 mm. It is apparent that the variations explored in this study significantly affect both the threshold current density and output power of the QCLs, although in general the IV characteristics are not changed much. It is interesting to note that the lasers with the highest threshold (21, 23, and 25) also happen to be the structures in which the quantum-well thickness is reduced (either through a reduction of all layers or a well reduction coinciding with a barrier increase). In preliminary modeling of the as-designed structures, there is no strong evidence to suggest there should be a significant degradation in laser performance. As such, it is hypothesized that the as-grown structure differs in an important way from the as-designed. Since the thinnest well layers are particularly important for carrier transport (they are in the injector and coupling well of the active region), this may be indicative of the existence of a critical thickness below which quality OMVPE growth may not result in the thin, deep, and square wells desired. Instead, those thin wells may be subject to effects of interface grading or similar effects, which create a well that is sloped and shallower than desired. However, further investigation into this result is required.

Utilizing the data of Fig. 2, the threshold field (the applied field at which the laser turns on) can be extracted. More rigorous analysis was performed on the laser turn-on characteristics using a model that solves the Schrodinger problem in a two-band k–p approximation. The as-measured period was used in the model to be consistent with the collected data. In the model, the turn-on is estimated by determining the applied field required for alignment of one of the lowest injector states with the upper laser state in the active region. The measured results and model outputs are summarized in Fig. 3; the model and data agree well. It is evident that these thickness changes can be responsible for as much as a 10 kV/cm change in threshold field, which corresponds to approximately a 2 V difference in threshold voltage for the 35-stage device investigated here. However, any trend beyond the one noted for threshold current in the previous paragraph does not seem apparent.

A summary of the electroluminescence data is presented in Fig. 4. It is apparent that the wavelength can be strongly influenced by these relatively small variations in layer thicknesses, spanning a range of nearly 1 μm. Comparison of the experimental results with the model shows excellent agreement in the trends. It is important to note that there is an absolute shift of approximately 0.6 μm between the experimental and calculated results; however, this trend has been anecdotally observed with OMVPE-grown QCLs and could be related to interface or compositional grading effects. An important result summarized in Fig. 4 is the strength of the wavelength shift with the different types of variations. It is observed that the effect of an increase or decrease in thickness of all layers has a relatively weak effect, with less than a 10 nm wavelength shift for a 1 Å change in individual layer thicknesses. In stark contrast, the complementary change in well and barrier thicknesses has a very strong effect, causing a 500 nm wavelength shift for a 1 Å change in layer thicknesses. It is worth noting that these are general best fit trends. The actual effect is not perfectly linear, as it is generally a complicated function of the layer thickness effects on eigenenergies, applied field, and other similar factors.

An intuitive explanation for this behavior begins by considering energy splitting of both the isolated single-well states and the super-states from the coupling of the single-well states. The mean position of the group of upper and lower active region states is approximately equal to the energy of the second and first energy level of an isolated well, respectively. Generally speaking, energy splitting of the individual well states is dictated by well thickness: thicker wells result in smaller energy splitting. Splitting of the super-states in each group is dictated by barrier thickness: thicker barriers result in smaller energy splitting. The upper laser state is generally the bottommost state of the upper active region group, and the lower laser state is the topmost of the lower active region group. Their separation is approximately equal to the energy splitting between lower and upper

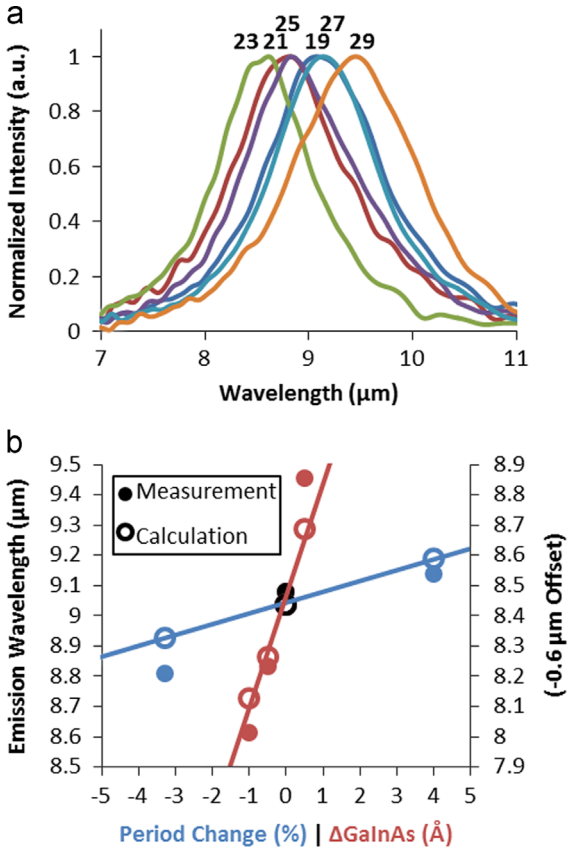

Fig. 4. Summary of the wavelength characteristics of the different QCLs of Table 1. (a) The electroluminescence spectra measure from mesa structures and (b) a comparison of the measured and calculated emission wavelength as a function of thickness change. Solid lines are included to guide the eye to the general trend for each type of thickness change.

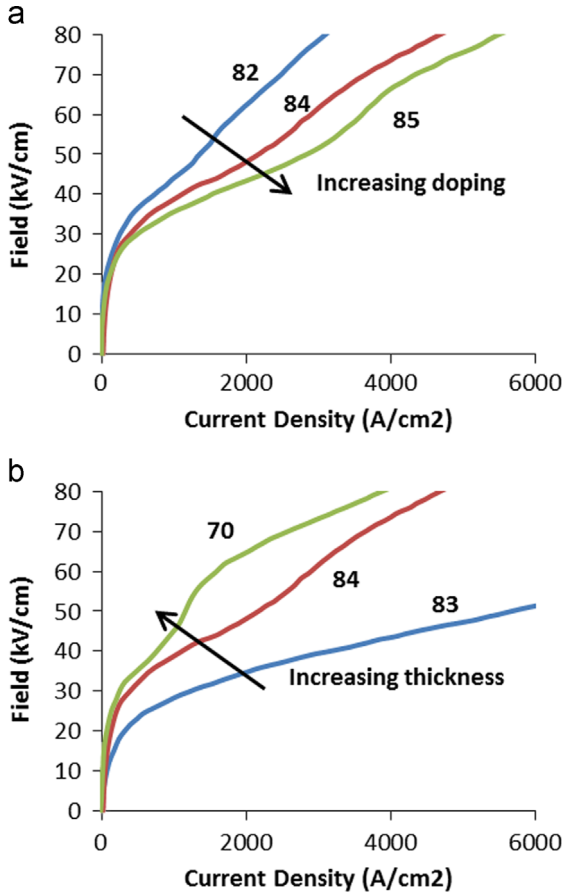

Fig. 5. Current voltage characteristics of a selection of the current transport test mesas. (a) Nominal thickness maintained and varied doping, and (b) nominal doping maintained and varied injection barrier thickness. The different sample numbers corresponding to the summary in Table 2 are labeled using their final two digits.

individual well states minus the amount they are moved up (lower state) and down (upper state) from that mean position by the coupling splitting. Thus, when both wells and barriers are made thicker, the effects tend to cancel, keeping the net splitting relatively unchanged. In contrast, when wells and barriers are changed complementarily, the effects move the laser energy states in opposite directions, increasing or decreasing the energy splitting depending on the type of thickness change. Although the same experimental study has not been applied to other QCL designs, this general explanation suggests that similar effects can be expected in different QCL structures. Further investigation is required to confirm this phenomenon and, in particular, to quantify its magnitude.

3.3. *Study 2 test mesas*

The voltage–current characteristics of a selection of the current transport test mesas of Table 2 are presented in Fig. 5. In particular, the characteristics for two cases are considered: (a) nominal injection barrier thickness (38 Å) and varied doping and (b) nominal doping (1.0×10^{17} cm^{-3}) and varied injection barrier thickness. As one might anticipate and similar to results found in Ref. [15], the effective resistance of the quantum-cascade structures tends to decrease as doping is increased or injection barrier thickness is decreased. The data suggest that injection barrier thickness has a stronger effect on current transport than the doping. However, results for cases where both doping and thickness were varied from the nominal (not presented here) are more ambiguous, and further investigation is required to fully understand the complexity of the combined doping and thickness effects on QCL carrier transport.

4. Summary

QCLs can be subject to a number of unintentional structure variations, such as thickness or doping changes, due to variability in the growth. This study explored the effects such variations might have on performance for OMVPE-grown QCLs. A number of important trends were observed. First, it was observed that structures in which the quantum wells were thinned seemed to have worse LI characteristics; this observation requires further investigation. Another notable trend is that complementary changes in well and barrier thicknesses have a very large effect on QCL wavelength, whereas simultaneous changes in thickness have a relatively weak effect; this phenomenon has been confirmed through an effective two-band k–p model. Finally, the effect of potentially the strongest influences on current transport, doping and injection barrier thickness, were investigated.

Acknowledgments

This work is sponsored by the Assistant Secretary of Defense for Research and Engineering under Air Force Contract FA8721-05-C-0002. Opinions, in- terpretations, conclusions and recommendations are those of the author and are not necessarily endorsed by the United States Government.

References

[1] J. Faist, F. Capasso, D.L. Silvco, C. Sirtori, A.L. Hutchinson, A.Y. Cho, Quantum cascade laser, Science 265 (1994) 553–556.

[2] M. Troccoli, D. Bour, S. Corzine, G. Hofler, A. Tandon, D. Mars, D. Smith, L. Diehl, F. Capasso, Low-threshold continuous-wave operation of quantum-cascade lasers grown by metalorganic vapor phase epitaxy, Appl. Phys. Lett. 85 (2004) 5842–5844.

[3] D. Bour, M. Troccoli, F. Capasso, S. Corzine, A. Tandon, D. Mars, G. Hofler, Metalorganic vapor-phase epitaxy of room-temperature low-threshold InGaAs/AlInAs quantum cascade lasers, J. Cryst. Growth 272 (2004) 526–530.

[4] C.A. Wang, R.K. Huang, A. Goyal, J.P. Donnelly, D.R. Calawa, S.G. Cann, F. O'Donnell, J.J. Plant, L.J. Missaggia, G.W. Turner, A. Sanchez-Rubio, OMVPE growth of highly strain-balanced GaInAs/AlInAs/InP for quantum cascade lasers, J. Cryst. Growth 210 (2008) 5191–5197.

[5] C.A. Wang, A. Goyal, R. Huang, J. Donnelly, D. Calawa, G. Turner, A. Sanchez-Rubio, A. Hsu, Q. Hu, B. Williams, Strain-compensated GaInAs/AlInAs/InP quantum cascade laser materials, J. Cryst. Growth 312 (2010) 1157–1164.

[6] A. Bismuto, R. Terazzi, M. Beck, J. Faist, Influence of the growth temperature on the performances of strain-balanced quantum cascade lasers, Appl. Phys. Lett. 98 (2011) 091105.

[7] Y. Huang, J.-H. Ryou, R.D. Dupuis, C. Pflugl, F. Capasso, K. Sun, A.M. Fischer, F. A. Ponce, Optimization of growth conditions for InGaAs/InAlAs/InP quantum cascade lasers by metalorganic chemical vapor deposition, J. Cryst. Growth 316 (2011) 75–80.

[8] C.A. Wang, D.R. Calawa, A. Goyal, S. Menzel, F. Capasso, Lattice-matched and strain-compensated materials for mid-wave and long-wave infrared quantum cascade lasers, ECS Trans. 41 (2011) 139–149.

[9] C.A. Wang, A.K. Goyal, S. Menzel, D.R. Calawa, M. Spencer, M.K. Connors, D. McNulty, A. Sanchez, G.W. Turner, F. Capasso, High power (>5 W) $\lambda \sim 9.6$ μm tapered quantum cascade lasers grown by OMVPE, J. Cryst. Growth 370 (2013) 212–216.

[10] G. Monastyrskyi, A. Aleksandrova, M. Elagin, M.P. Semtsiv, W.T. Masselink, V. Bryksa, Correlation of the MBE growth temperature, material quality, and performance of quantum cascade lasers, J. Cryst. Growth 378 (2013) 614–617.

[11] K. Fujita, S. Furuta, A. Sugiyama, T. Ochiai, T. Edamura, N. Akikusa, M. Yamanishi, H. Kan, High-performance $\lambda \sim 8.6$ μm quantum cascade lasers with single phonon-continuum depopulation structures, IEEE J. Quant. Electron. 46 (2010) 683–688.

[12] R.F. Kazarinov, R.A. Suris, Possibility of the amplification of electromagnetic waves in a semiconductor with a superlattice, Sov. Phys. Semicond. 5 (1971) 707–709.

[13] R.F. Kazarinov, R.A. Suris, Electric and electromagnetic properties of semiconductors with a superlattice, Sov. Phys. Semicond. 6 (1972) 120–131.

[14] C. Sirtori, F. Capasso, J. Faist, A.L. Hutchinson, D.L. Sivco, A.Y. Cho, Resonant tunneling in quantum cascade lasers, IEEE J. Quant. Electron. 34 (1998) 1722–1729.

[15] S.S. Howard, D.P. Howard, K. Franz, A. Hoffman, D.L. Sivco, C.F. Gmachl, The effect of injector barrier thickness and doping level on current transport and optical transition width in a $\lambda \sim 8.0$ μm quantum cascade structure, Appl. Phys. Lett. 93 (2008) 191107.